CHEMISTRY OF MATERIALS

Article

pubs.acs.org/cm

Significant Improvement of Dye-Sensitized Solar Cell Performance Using Simple Phenothiazine-Based Dyes

Yong Hua,[†,⊥] Shuai Chang,[‡,⊥] Dandan Huang,[§] Xuan Zhou,[†] Xunjin Zhu,*[,†,∥] Jianzhang Zhao,[§] Tao Chen,*[,‡] Wai-Yeung Wong,*[,†,§,∥] and Wai-Kwok Wong*[,†,∥]

[†]Institute of Molecular Functional Materials, Department of Chemistry and Institute of Advanced Materials, Hong Kong Baptist University, Waterloo Road, Kowloon Tong, Hong Kong, P. R. China

[‡]Department of Physics, The Chinese University of Hong Kong, Shatin, New Territories, Hong Kong, P. R. China

[§]State Key Laboratory of Fine Chemicals, School of Chemical Engineering, Dalian University of Technology, Dalian, 116024, P. R. China

[∥]HKBU Institute of Research and Continuing Education, Shenzhen Virtual University Park, Shenzhen, 518057, P. R. China

Supporting Information

ABSTRACT: A series of simple phenothiazine-based dyes have been synthesized, in which a cyanoacrylate acceptor directly attached to the C(3) position of phenothiazine, and an additional linear electron-rich (4-hexyloxy)-phenyl group at C(7) on the opposite side of the acceptor, and an alkyl chain with different length at N(10) of the phenothiazine periphery are presented. The dye molecules have a linear shape which is favorable for the formation of a compact dye layer on the TiO_2 surface, while their butterfly conformations can sufficiently inhibit molecular aggregation. Moreover, the structural features of (4-hexyloxy)phenyl donor moiety at the C(7) position of phenothiazine extends the π-conjugation of the chromophore, thus enhancing the performance of dye-sensitized solar cells (DSSCs). Moreover, the alkyl substituents with different chain length at the N(10) atom of phenothiazine could further optimize the performance through completely shielding the surface of TiO_2 from the I^-/I^{3-} electrolyte and subsequently reducing the leakage of dark current. Under simulated AM 1.5G irradiation, the PT-C6 based DSSC produces a short-circuit photocurrent of 15.32 mA cm^{-2}, an open-circuit photovoltage of 0.78 V, a fill factor of 0.69, corresponding to a power conversion efficiency (PCE) of 8.18%, which exceeds the reference N719 (7.73%) under identical fabrication conditions. Notably, the designed molecular structure represents the highest photovoltaic conversion efficiency value when compared with other reported phenothiazine-derived dyes.

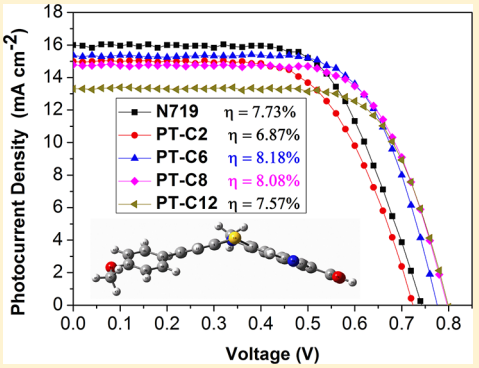

KEYWORDS: *phenothiazine, dye-sensitized solar cells, π-conjugation, aggregation, charge recombination*

INTRODUCTION

Conversion of solar energy into electricity will play a substantial role in meeting the rising demand for energy. Dye-sensitized solar cells (DSSCs), comprising chromophores, redox shuttles, and nanoporous semiconductors, have been intensively investigated since the pioneering work of O'Regan and Grätzel in 1991,[1] because they are regarded as promising alternatives to silicon photovoltaic devices.[2] The rise of the energy conversion limit is always dependent on the development of new dyes, as well as new electrolytes,[3−5] which leads to the PCE increasing from 11% to 12.3% in a recent report.[6] In particular, the design and synthesis of donor-π-acceptor metal-free organic dyes has led to a number of efficient sensitizers for DSSCs.[7−14] However, it is known that most organic sensitizers possess a rod-shape configuration, and they are inclined to form aggregates on the semiconductor surface, leading to lower photovoltaic performance in DSSCs than N719 because of intermolecular quenching of molecules residing in the system not functionally attached to the TiO_2 surface and thus acting as filters.[15] It is worth noting that a phenothiazine-based dye contains electron-rich nitrogen and sulfur heteroatoms in a heterocyclic structure with high electron-donating ability, and its nonplanar butterfly conformation can sufficiently inhibit molecular aggregation and the formation of intermolecular excimers.[16,17] Meanwhile, the 10-substituent on N can further enhance the charge separation at the oxide solution interface. Furthermore, the two phenyl groups are arranged in a small torsion angle related to N(10) and S(9) atoms, so that π-delocalization can be extended over the entire chromophore. The structural features of phenothiazine-based dye make it a promising type of sensitizers for DSSCs. Recently, a diversity of strategies have been utilized to extend the range of π-electron delocalization and increase the molar absorptivity of the materials.[18−28] For example, the addition of thiophene and

Received: March 11, 2013
Revised: April 22, 2013

   dx.doi.org/10.1021/cm400800h | *Chem. Mater.* XXXX, XXX, XXX−XXX

triarylamine moieties in some of the structures extends π-conjugation of the chromophore and increases the molar absorptivity of the materials, meanwhile, this makes the whole molecule occupy a larger surface area than a molecule of linear shape, leading to the reduction of dye loading capacity.[17] At the same time, the molecular engineering of sensitizers can enhance the charge separation at the oxide solution interface.[22] As a result, certain structural modifications of this kind of dye give moderate improvement of the PCEs. Also, the development of new phenothiazine-based dyes encourages further structural optimization of such low-cost organic dyes, boosting the practical application of DSSCs.

In this article, a series of new simple organic dyes (**PT-C*n***, *n* = 2, 6, 8, 12) based on the phenothiazine unit were synthesized (Figure 1), in which a cyanoacrylate moiety was added at the

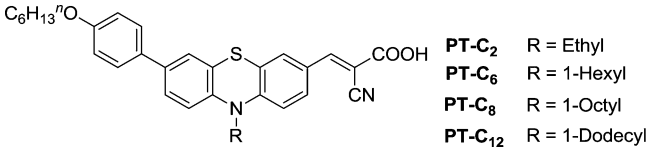

Figure 1. Structures of dyes **PT-C*n*** (*n* = 2, 6, 8, 12).

C(3) position of the phenothiazine ring as an electron acceptor, a (4-hexyloxy)phenyl group at the C(7) atom as an electron donor on the opposite side, and an alkyl chain with different lengths at the N(10) atom of phenothiazine as a block against the electrolyte. Instead of appending with the nonplanar bulky triarylamine with good electron-donating and -transporting capability, the linear planar 4-hexyloxyphenyl donor group together with the electron-rich phenothiazine moiety provides a satisfied relay for the electron migration from donor to acceptor. Also, the dye molecules with linear shapes are favorable for the formation of a compact sensitizer layer, while their butterfly conformations can sufficiently inhibit molecular aggregation. Moreover, the linear *N*-alkyl substituent is also beneficial. The molecular design strategy was demonstrated here to effectively improve the photovoltaic performance with the best power conversion efficiency up to 8.18%, which exceeds the reference Ru(II)-based N719 dye (7.76%) in parallel investigations.

EXPERIMENTAL SECTION

Materials and Reagents. All solvents and reagents were purchased from Sigma-Aldrich Company and used as received without further purification. The starting material phenothiazine and 2-cyanoacetic acid were purchased commercially. The intermediates **1a−1d**, **2a−2d**, and **3a−3d** were prepared according to the literature methods reported[16,17] and characterized by comparing their ^{1}H NMR and ^{13}C NMR spectra with those found in the literature. Dye *cis*-bis(isothiocyanato)bis(2,2′-bipyridyl-4,4′-dicarboxylato)-ruthenium-(II)-bis-tetrabutyl-ammonium, (coded as N719), TiO_2 paste, and iodide-based liquid electrolyte (HL-HPE) were purchased from Dyesol company. The synthetic routes of phenothiazine-based dyes **PT-C*n*** are outlined in Scheme 1, and the details are depicted as follows.

*General Synthetic Procedure for **4a−d**.* A mixture of **3a−3d** (0.30 mmol), (4-(hexyloxy)phenyl)boronic acid (89 mg, 0.40 mmol), $Pd(PPh_3)_4$ (25 mg, 0.04 mmol), and 2 N aqueous solution of K_2CO_3 (2 mL) in THF (10 mL) was heated to reflux under a N_2 atmosphere for about 12 h. Then, the solvent was removed under vacuum and the residue was purified by column chromatography on silica gel using a 1:4 mixture of hexane and CH_2Cl_2 as eluent to afford **4a−4d** as red solids, respectively.

4a. 100 mg, 77% yield. ^{1}H NMR (400 MHz, $CDCl_3$): δ (ppm) 9.72 (s, 1H), 7.55−7.58 (m, 1H), 7.49 (d, *J* = 2.0 Hz, 1H), 7.40 (t, *J* = 2.0 Hz, 1H), 7.39 (t, *J* = 2.0 Hz, 1H), 7.32−7.35 (m, 2H), 6.95 (t, *J* = 2.0 Hz, 2H), 6.93 (t, *J* = 2.0 Hz, 2H), 3.97 (t, *J* = 6.8 Hz, 2H), 3.95 (t, *J* = 6.8 Hz, 2H), 1.70−1.75 (m, 2H), 1.36−1.42 (m, 2H), 1.31−1.34 (m, 7H), 0.88 (t, *J* = 7.2 Hz, 3H). ^{13}C NMR (400 MHz, $CDCl_3$): δ (ppm) 190.03, 158.72, 151.52, 142.42, 136.57, 131.95, 130.97, 129.10, 128.45, 127.50, 126.89, 125.87, 125.60, 125.35, 116.89, 115.46, 114.77, 51.49, 36.01, 31.64, 30.28, 25.74, 23.55, 14.19, 14.07. HRMS (MALDI-TOF, *m*/*z*): [M$^+$] calcd for ($C_{27}H_{29}NO_2S$) 431.1934; found, 431.1937.

4b. 115 mg, 78% yield. ^{1}H NMR (400 MHz, $CDCl_3$): δ (ppm) 9.71 (s, 1H), 7.54−7.57 (m, 1H), 7.51 (d, *J* = 2.0 Hz, 1H), 7.35−7.37 (m, 2H), 7.22−7.25 (m, 1H), 7.21 (d, *J* = 2.0 Hz, 1H), 6.83−6.87 (m, 2H), 6.83 (d, *J* = 2.0 Hz, 1H), 6.81 (d, *J* = 2.0 Hz, 1H), 3.92 (t, *J* = 6.8 Hz, 2H), 3.83 (t, *J* = 6.8 Hz, 2H), 1.70−1.75 (m, 4H), 1.28−1.39 (m, 4H), 1.18−1.20 (m, 8H), 0.79−0.86 (m, 6H). ^{13}C NMR (400 MHz, $CDCl_3$): δ (ppm) 190.01, 158.75, 150.58, 141.92, 136.50, 131.91, 130.97, 130.16, 128.43, 127.52, 125.68, 125.47, 124.60, 124.03, 116.07, 114.86, 114.65, 48.09, 31.61, 31.41, 29.27, 26.73, 26.55, 25.75, 22.63, 22.60, 14.15, 14.06, 13.99. HRMS (MALDI-TOF, *m*/*z*): [M$^+$] calcd for ($C_{31}H_{37}NO_2S$) 487.2599; found, 487.2587.

4c. 116 mg, 75% yield. ^{1}H NMR (400 MHz, $CDCl_3$): δ (ppm) 9.78 (s, 1H), 7.61−7.66 (m, 1H), 7.57 (d, *J* = 2.0 Hz, 1H), 7.42 (d, *J* = 2.0 Hz, 1H), 7.28−7.33 (m, 2H), 7.09−7.18 (m, 1H), 6.95 (t, *J* = 2.0 Hz,

Scheme 1. Synthesis of Phenothiazine-Based Dyes PT-C*n* (*n* = 2, 6, 8, 12)

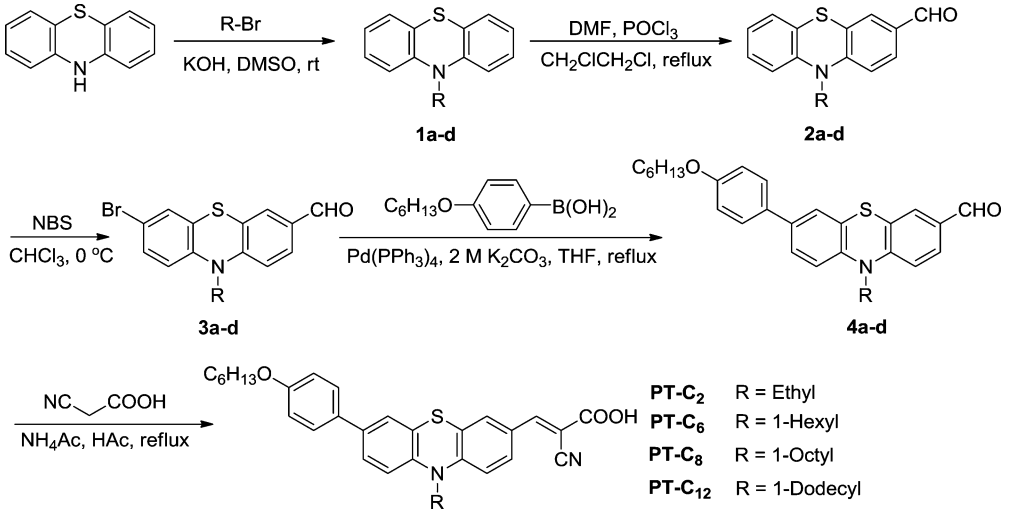

dx.doi.org/10.1021/cm400800h | *Chem. Mater.* XXXX, XXX, XXX−XXX

2H), 6.86 (t, J = 2.0 Hz, 2H), 3.96 (t, J = 6.8 Hz, 2H), 3.88 (t, J = 6.8 Hz, 2H), 1.77−1.84 (m, 4H), 1.41−1.46 (m, 4H), 1.25−1.39 (m, 12H), 0.85−0.89 (m, 6H). ^{13}C NMR (400 MHz, $CDCl_3$): δ (ppm) 190.01, 158.72, 150.54, 141.88, 131.88, 130.94, 130.16, 130.07, 128.38, 127.55, 127.50, 125.66, 124.00, 123.56, 116.06, 115.94, 114.64, 68.10, 48.07, 36.09, 31.74, 31.63, 29.28, 29.18, 26.85, 26.75, 25.77, 23.99, 22.64, 14.13, 14.09. HRMS (MALDI-TOF, m/z): [M^+] calcd for ($C_{33}H_{41}NO_2S$) 515.2989; found, 515.2977.

4d. 124 mg, 68% yield. ^{1}H NMR (400 MHz, $CDCl_3$): δ (ppm) 9.78 (s, 1H), 7.62−7.64 (m, 1H), 7.58 (d, J = 4.0 Hz, 1H), 7.44 (d, J = 4.0 Hz, 1H), 7.42 (d, J = 4.0 Hz, 1H), 7.31−7.34 (m, 1H), 7.28 (d, J = 4.0 Hz, 1H), 6.92 (t, J = 4.0 Hz, 2H), 6.88 (t, J = 4.0 Hz, 2H), 3.98 (t, J = 6.8 Hz, 2H), 3.89 (t, J = 6.8 Hz, 2H), 1.79−1.87 (m, 4H), 1.45−1.59 (m, 4H), 1.37−1.42 (m, 4H), 1.29−1.35 (m, 16H), 0.85−0.89 (m, 6H). ^{13}C NMR (400 MHz, $CDCl_3$): δ (ppm) 189.99, 158.72, 150.56, 141.89, 136.47, 131.88, 130.94, 130.16, 128.41, 127.50, 125.65, 125.45, 124.56, 124.01, 123.56, 116.06, 114.83, 68.12, 48.08, 31.94, 31.78, 31.65, 31.05, 29.65, 29.54, 29.37, 29.28, 29.22, 26.85, 26.74, 25.77, 22.72, 22.65, 14.17, 14.09. HRMS (MALDI-TOF, m/z): [M^+] calcd for ($C_{37}H_{49}NO_2S$) 571.3588; found, 571.3587.

General Synthetic Procedure for Dyes ***PT-Cn*** *(n = 2, 6, 8, 12).* A mixture of precursor **4a**−**4d** (0.23 mmol) and cyanoacetic acid (89 mg, 1.10 mmol) in acetic acid (20 mL) was refluxed in the presence of ammonium acetate (200 mg) overnight under a N_2 atmosphere. Then, water was added and extracted with CH_2Cl_2. Next, the solvent was removed under vacuum and the crude compound was purified by column chromatography on silica gel eluting with CH_2Cl_2/MeOH (20:1, v/v) to give **PT-C*n*** as a dark red solid.

PT-C2. 74 mg, 61.5% yield. ^{1}H NMR (400 MHz, DMSO-d_6): δ (ppm) 8.17 (s, 1H), 7.91−7.94 (m, 1H), 7.82 (d, J = 2.0 Hz, 1H), 7.57 (s, 2H), 7.55 (s, 2H), 7.15 (d, J = 8.8 Hz, 1H), 7.10 (d, J = 8.8 Hz, 1H), 6.96−7.00 (t, J = 8.8 Hz, 2H), 4.02 (t, J = 6.8 Hz, 2H), 3.97 (t, J = 6.8 Hz, 2H), 1.70−1.73 (m, 2H), 1.36−1.42 (m, 2H), 1.31−1.34 (m, 7H), 0.88 (t, J = 6.8 Hz, 3H). ^{13}C NMR (400 MHz, DMSO-d_6): δ (ppm) 163.79, 158.23, 152.47, 147.99, 140.59, 135.22, 131.77, 130.68, 128.86, 127.14, 125.48, 125.34, 124.38, 121.90, 121.73, 116.82, 116.20, 114.99, 114.80, 99.25, 41.76, 30.99, 30.68, 28.63, 25.18, 22.07, 13.91, 12.26. HRMS (MALDI-TOF, m/z): [M^+] calcd for ($C_{30}H_{30}N_2O_3S$) 498.1971; found, 498.2017.

PT-C6. 55 mg, 66% yield. ^{1}H NMR (400 MHz, $CDCl_3$): δ (ppm) 8.07 (s, 1H), 7.88−7.91 (m, 1H), 7.66 (d, J = 2.0 Hz, 1H), 7.42−7.44 (m, 2H), 7.30−7.32 (m, 1H), 7.25 (t, J = 2.0 Hz, 1H), 6.94 (d, J = 2.0 Hz, 1H), 6.93 (d, J = 2.0 Hz, 1H), 6.83−6.89 (m, 2H), 4.00 (t, J = 6.8 Hz, 2H), 3.88 (t, J = 6.8 Hz, 2H), 1.75−1.86 (m, 4H), 1.45−1.47 (m, 4H), 1.32−1.37 (m, 8H), 0.92 (t, J = 6.8 Hz, 6H). ^{13}C NMR (400 MHz, $CDCl_3$): δ (ppm) 168.18, 158.84, 154.63, 150.04, 141.15, 136.39, 132.01, 131.73, 130.50, 127.49, 125.70, 125.40, 125.21, 124.25, 123.45, 116.04, 115.87, 114.92, 114.78, 97.28, 68.18, 48.22, 34.50, 31.60, 31.39, 29.26, 26.68, 26.52, 25.74, 22.61, 14.02, 13.96. HRMS (MALDI-TOF, m/z): [M^+] calcd for ($C_{34}H_{38}N_2O_3S$) 554.2598; found, 554.2580.

PT-C8. 59 mg, 74% yield. ^{1}H NMR (400 MHz, $CDCl_3$): δ (ppm) 8.04 (s, 1H), 7.86 (d, J = 8.4 Hz, 1H), 7.62 (d, J = 8.4 Hz, 1H), 7.41 (d, J = 8.4 Hz, 2H), 7.28−7.31 (m, 1H), 7.21 (d, J = 8.4 Hz, 1H), 6.92 (d, J = 8.4 Hz, 2H), 6.79−6.86 (m, 2H), 3.97 (t, J = 6.4 Hz, 2H), 3.83 (t, J = 6.4 Hz, 2H), 1.75−1.82 (m, 4H), 1.42−1.56 (m, 4H), 1.33−1.35 (m, 4H), 1.26−1.32 (m, 8H), 0.85−0.90 (m, 6H). ^{13}C NMR (400 MHz, $CDCl_3$): δ (ppm) 168.76, 158.80, 154.74, 150.24, 142.67, 141.00, 136.68, 132.16, 131.64, 130.40, 127.47, 125.67, 125.29, 124.01, 123.26, 116.02, 115.91, 114.89, 114.71, 97.71, 48.23, 48.15, 31.75, 31.63, 29.28, 29.25, 29.19, 26.85, 26.67, 26.62, 25.77, 22.65, 14.14, 14.10. HRMS (MALDI-TOF, m/z): [M^+] calcd for ($C_{36}H_{42}N_2O_3S$) 583.2988; found, 583.2987.

PT-C12. 62 mg, 77% yield. ^{1}H NMR (400 MHz, $CDCl_3$): δ (ppm) 8.07 (s, 1H), 7.89 (s, 1H), 7.66 (d, J = 8.8 Hz, 1H), 7.42 (d, J = 8.8 Hz, 2H), 7.25 (d, J = 8.8 Hz, 1H), 7.24 (d, J = 8.8 Hz, 1H), 6.89 (t, J = 8.8 Hz, 2H), 6.83−6.87 (m, 2H), 3.98 (t, J = 6.6 Hz, 2H), 3.87 (t, J = 6.4 Hz, 2H), 1.77−1.83 (m, 4H), 1.43−1.47 (m, 4H), 1.24−1.37 (m, 20H), 0.85−0.92 (m, 6H). ^{13}C NMR (400 MHz, $CDCl_3$): δ (ppm) 168.53, 158.81, 154.72, 150.06, 142.73, 141.98, 141.09, 136.77, 132.11, 130.50, 127.50, 125.71, 125.54, 123.92, 123.37, 116.18, 116.06, 115.16, 114.88, 97.14, 48.21, 31.94, 31.62, 29.63, 29.57, 29.54, 29.37, 29.27, 29.16, 26.83, 26.74, 26.66, 26.56, 25.76, 22.72, 22.64, 14.16, 14.08. HRMS (MALDI-TOF, m/z): [M^+] calcd for ($C_{40}H_{50}N_2O_3S$) 638.3536; found, 638.3552.

Characterizations. ^{1}H and ^{13}C NMR spectra were recorded with a Bruker Ultrashield 400 Plus NMR spectrometer. The UV−visible absorption spectra of these dyes were measured in CH_2Cl_2 solution with a Varian Cary 100 UV−vis spectrophotometer. Emission spectra were performed using a Photon Technology International (PTI) Alphascan spectrofluorimeter. High-resolution matrix-assisted laser desorption/ionization time-of-flight (MALDI-TOF) mass spectra were obtained with a Bruker Autoflex MALDI-TOF mass spectrometer. The cyclic voltammograms (CV) were measured with Versastat II electrochemical workstation using a normal three-electrode cell with a Pt working electrode, a Pt wire counter electrode, and a Ag/Ag^+ reference electrode. The supporting electrolyte was 0.1 M tetra-*n*-butylammonium hexafluorophosphate in CH_2Cl_2 solution. The potential of the reference electrode was calibrated by ferrocene after each set of measurements, and all potentials mentioned in the work were against the normal hydrogen electrode.

Fabrication and Characterization of Cells. To make a reasonable comparison, all the anode films for the DSSCs were made under the same standard manner, which are composed of a 12 μm thick of transparent layer (TiO_2 with diameter of 20 nm) and 6 μm thick of scattering layer (TiO_2 nanoparticles with a diameter of 200 nm). Specifically, a doctor-blade technique was utilized to prepare photoanode (TiO_2) films. First, a layer of ∼6 μm TiO_2 paste (20 nm) was doctor-bladed onto the FTO conducting glass and then relaxed at room temperature for 3 min before heating at 150 °C for 6 min; this procedure was repeated once to achieve a film thickness of ∼12 μm and the resulting surface was finally coated by a scattering layer (∼6 μm) of TiO_2 paste (200 nm). The electrodes were gradually heated under an air flow at 275 °C for 5 min, 325 °C for 5 min, 375 °C for 5 min, and 470 °C for 30 min to remove polymers and generate a three-dimensional TiO_2 nanoparticle network. After that, the sintered films were soaked with 0.02 M TiF_4 aqueous solution for 45 min at 70 °C, washed with deionized water, and further annealed at 450 °C for 30 min. After cooling down to ∼80 °C, the electrodes were immersed into a 5 × 10^{-4} M dye bath in CH_2Cl_2 solution for the **PT-C*n*** dye series or in acetonitrile/*tert*-butyl alcohol (volume ratio, 1:1) for N719 dye and maintained in the dark for 16 h. Afterward, the electrodes were rinsed with ethanol to remove the nonadsorbed dyes and dried in the air. Pt counter electrodes were prepared by sputtering method at 15 mA for 90 s at a power of 150 W. Two holes (0.75 mm in diameter) were predrilled in the FTO glass for introducing the electrolyte. The dye-adsorbed TiO_2 electrode and Pt-counter electrode were assembled into a sandwich type cell and sealed with a hot-melt parafilm at about 100 °C. The liquid electrolyte consisting of 0.6 M 1,2-dimethyl-3-propylimidazolium iodide (DMPII), 0.1 M LiI, 0.05 M I_2 in a mixture of acetonitrile and 4-*tert*-butylpyridine (volume ratio, 1:1) was introduced into the cell through the drilled holes at the back of the counter electrode. At last, the holes were sealed by parafilm and covering glass (0.1 mm thickness) at elevated temperature. The effective areas of all the TiO_2 electrodes were 0.24 cm^2. The current−voltage (J−V) characteristics of the assembled DSSCs were measured by a semiconductor characterization system (Keithley 236) at room temperature in air under the spectral output from solar simulator (Newport) using an AM 1.5G filter with a light power of 100 mW/cm^2. IPCEs of DSSCs were recorded in the Solar Cell QE/IPCE Measurement System (Zolix Solar Cell Scan 100) using dc mode. CHI 660D electrochemical workstation was used to characterize the electrochemical properties of the DSSCs. Electrochemical impedance spectroscopy (EIS) was recorded under dark conditions over a frequency range of 0.1−10^5 Hz with an ac amplitude of 10 mV, and the parameters were calculated from Z-View software (v2.1b, Scribner AssociatNe, Inc.). For the open-circuit voltage decay measurements, the cell was first illuminated for 20 s to a steady voltage, then the illumination was turned off for 80 s and the open-circuit voltage decay curve was recorded.

dx.doi.org/10.1021/cm400800h | *Chem. Mater.* XXXX, XXX, XXX−XXX

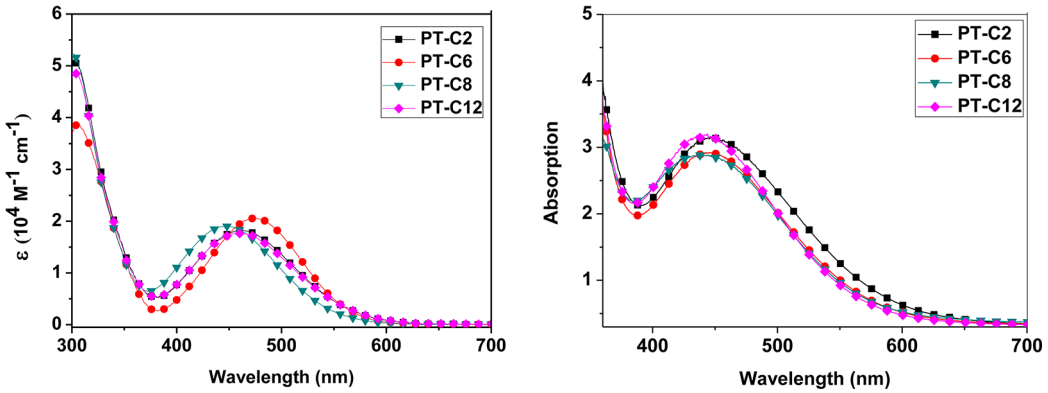

Figure 2. Absorption spectra of the new dyes in CH_2Cl_2 solution (left) and on TiO_2 films (right).

Table 1. Absorption and Electrochemical Parameters for the New Dyes

dye	λ_{max} ($\varepsilon \times 10^4$ M^{-1} cm^{-1})[a]/nm	λ_{max}[b]/nm	E_{ox}[c]/V	E_{0-0}[d]/eV	E_{ox*}[e]/V
PT-C2	464 (1.82), 302 (5.23)	444	0.61	2.18	−1.57
PT-C6	474 (2.06), 302 (4.82)	448	0.62	2.19	−1.57
PT-C8	449 (1.90), 303 (5.23)	439	0.67	2.12	−1.45
PT-C12	458 (1.77), 304 (2.94)	445	0.70	2.10	−1.40

[a]Absorption maximum in 1×10^{-5} mol L^{-1} CH_2Cl_2 solution. [b]Absorption maximum on TiO_2 film. [c]Oxidation potential in CH_2Cl_2 solution containing 0.1 M $(n\text{-}C_4H_9)_4NPF_6$ with a scan rate of 100 mV s^{-1} (vs NHE). [d]E_{0-0} was determined from the onset of absorption spectrum. [e]$E_{ox*} = E_{ox} - E_{0-0}$.

RESULTS AND DISCUSSION

Synthesis and Characterization of Dyes. The synthesis of **PT-C*n*** follows the previously reported strategy of a Suzuki cross coupling of (4-(1-hexyloxy)phenyl)boronic acid with 7-bromo-*N*-hexyl-10*H*-phenothiazine-3-carbaldehyde and its analogues, respectively, followed by the widely employed Knoevenagel condensation to construct the classical donor-π-acceptor dyes. All the new compounds were characterized by their ^{1}H NMR, ^{13}C NMR, and MALDI-TOF mass spectral data.

UV−Visible Absorption Properties. The UV−vis absorption spectra of all dyes in CH_2Cl_2 solutions and adsorbed on TiO_2 films have been recorded (Figure 2), and the detailed spectroscopic data are summarized in Table 1. All of these dyes exhibit two major distinct broad absorption bands in the range of 300−600 nm. The shorter wavelengths located at 300−370 nm are ascribed to the aromatic $\pi-\pi^*$ electronic transitions of the chromophores, while the longer wavelengths located at 380−600 nm are attributed to the intramolecular charge transfer (ICT) from the donor to the acceptor, providing efficient charge-separation at the excited state. Because of the very simple donor−π−acceptor structures based on phenothiazine, these dyes show relatively low molar extinction coefficient (ε) with values of around 20 000 M^{-1} cm^{-1}, which are still higher than those of standard ruthenium dyes N3 and N719 (13 900 and 14 000 M^{-1} cm^{-1}, respectively).[29] Also, the molar extinction coefficients of these dyes for the visible absorption peaks are in the order of **PT-C6** > **PT-C8** > **PT-C12** > **PT-C2**. The results indicate that the linear 1-hexyl group at N(10) gives a simple and balanced structure and better absorption of light, which favors the light harvesting and hence photocurrent generation in DSSCs. When these dyes are adsorbed onto the nanocrystalline TiO_2 films, the absorption bands display a slight blue-shift with respect to those in solutions, which can be mainly ascribed to the deprotonation of carboxylic acid.[30−32]

Electrochemical Properties. To fabricate an efficient DSSC, besides the light-harvesting yield of a dye-coated TiO_2, it is also of much pertinence that there are favorable energy-offsets of the dye molecules with respect to the TiO_2 nanocrystals and redox electrolytes. Here, the electrochemical behaviors of these dyes were monitored by cyclic voltammetry (Figure 3). The ground oxidation potentials (E_{ox}) correspond

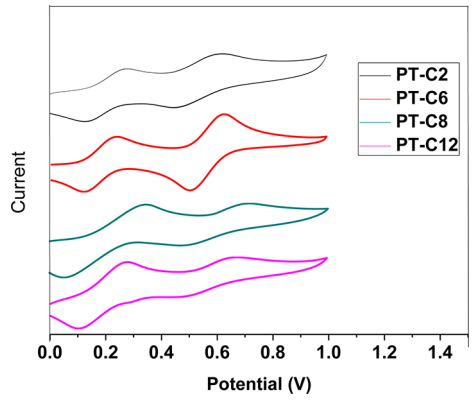

Figure 3. Cyclic voltammograms of dyes **PT-C*n*** in CH_2Cl_2 solution.

to the highest occupied molecular orbitals (HOMO). The lowest unoccupied molecular orbitals (LUMO) were obtained from the values of E_{ox} and the zero−zero band gaps (E_{0-0}) estimated from the onset of the UV−visible absorption spectra (Table 1). The HOMO levels of all dyes are more positive than iodide/tri-iodide redox potential value (0.4 V vs NHE), which indicates the oxidized dyes could be efficiently regenerated by the electrolyte. It is found that increasing the length and steric hindrance of the alkyl chain at N(10) can lift the HOMO energy levels from 0.61 V of **PT-C2** to 0.70 V of **PT-C12** and 0.70 V of **PT-C8**. The larger difference between iodide/tri-iodide potential and the HOMO level, the more efficient the

dx.doi.org/10.1021/cm400800h | *Chem. Mater.* XXXX, XXX, XXX−XXX

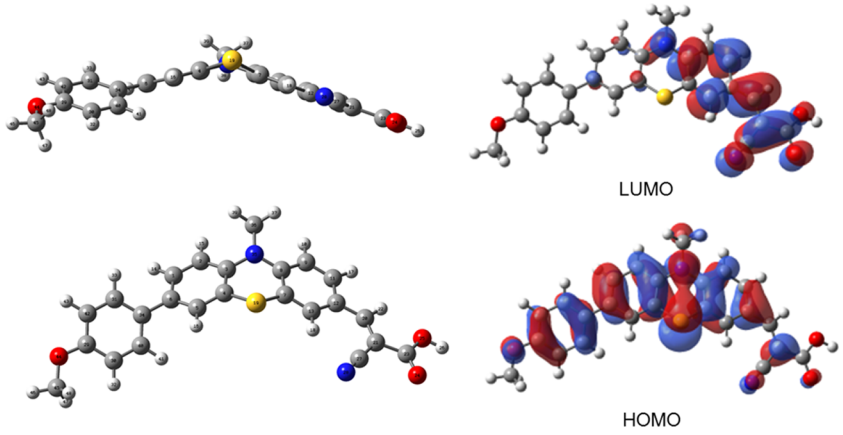

Figure 4. Optimized ground state geometry (left) and frontier molecular orbitals of the HOMO and LUMO (right) calculated by DFT on a B3LYP/6-31 t G (d)* level.

dye regeneration, which can effectively avoid the geminate charge recombination between oxidized dye molecules and photoinjected electrons in the TiO_2 film, and may result in a higher short-circuit photocurrent (J_{sc}) and open-circuit photovoltage (V_{oc}). On the other hand, the LUMO levels of all dyes are more negative than the conduction band edge (CB) of TiO_2 (−0.5 V vs NHE), providing the possibility of electron injection from the excited dye molecules to the conduction band of TiO_2.[33] Specifically, the higher LUMO levels of dyes **PT-C2** and **PT-C6** are favorable for faster electron injection into TiO_2, thus suppressing back reactions.

Theoretical Calculations. The structures of dyes have been further analyzed by using B3LYP/6-31G(d)* hybrid functional for full geometrical optimization (Figure 4). In the ground state, the geometry of phenothiazine is not totally planar but is rather slightly bent in the middle to give a butterfly shape. That is, the angle between the two terminal phenyl rings is 146° from the nitrogen side, while the cyanoacrylic acid functionality is in-plane with the substituted phenyl ring of phenothiazine. The nonplanar shape of the phenothiazine ring reveals the nonaromatic character of the central heterocycle, which can suppress dye-aggregation and reduce the rate of internal charge recombination, thus increasing the efficiency of solar cells. The charge distribution in the frontier molecular orbitals can be depicted in Figure 4 (right). Because of a relatively smaller dihedral angle of about 35° between the phenothiazine core and the (4-hexyloxy)phenyl group, the HOMO levels are delocalized throughout the entire system, while the LUMO lies mainly on cyanoacrylic acid acceptor and partly on the neighboring phenothiazine core, which would have a favorable effect on the electronic transition from the HOMO to the LUMO. The sufficient orbital overlap between donor and acceptor suggests a fast charge transition. When these dyes are adsorbed on the nanocrystalline TiO_2 surface, the photoinduced electron can be effectively injected into the conduction band of TiO_2 semiconductor from the donor unit via the terminal cyanoacrylic acid acceptor. This further demonstrates that the cyanoacrylic acid group attached directly to the C(3) atom of phenothiazine as an electron acceptor can effectively drive electron injection from the LUMO state of the dye to the TiO_2 conduction band.

Photovoltaic Performance. A series of DSSCs have been fabricated as described in the Experimental Section and tested under standard conditions (AM 1.5G, 100 mW cm^{-2}) in order to investigate the photovoltaic performance of the dyes. The parameters of DSSCs fabricated with these dyes, i.e., short-circuit current density (J_{sc}), open-circuit photovoltage (V_{oc}), fill factor (FF), and total power conversion efficiency (η) are summarized in Table 2, and the photocurrent−voltage (J−V) plots are shown in Figure 5. Among these dyes, the cell based on **PT-C6** exhibits the highest η of 8.18% (J_{sc} = 15.32 mA cm^{-2}, V_{oc} = 0.775 V, FF = 0.689), which exceeds the efficiency of an **N719**-based device (7.73%) fabricated under the same working conditions. To the best of our knowledge, the η of 8.18% is the highest value among previously reported DSSCs based on phenothiazine-type dyes, which can be mainly

Table 2. Photovoltaic Parameters of DSSCs under Full Sunlight Illumination (AM 1.5G, 100 mW cm^{-2})[a]

dye	J_{sc}/mA cm^{-2}	V_{oc}/V	FF	η/%	R_{rec}/Ω cm^{-1}
PT-C2	14.97	0.723	0.635	6.87	154.58
PT-C6	15.32	0.775	0.689	8.18	468.11
PT-C8	14.75	0.797	0.687	8.08	649.81
PT-C12	13.31	0.799	0.712	7.57	969.60
N719	15.98	0.741	0.653	7.73	121.84

[a]Performance of DSSCs measured in a 0.24 cm^2 working area on a FTO substrate at room temperature. Dyes were maintained at 0.5 mM in CH_2Cl_2 solution for **PT-Cn** dyes and in acetonitrile/*tert*-butyl alcohol (1:1, v/v) for **N719**. Electrolyte: LiI (0.05 M), I_2 (0.1 M), and DMPII (0.6 M) in acetonitrile/*tert*-butyl alcohol (1:1, v/v).

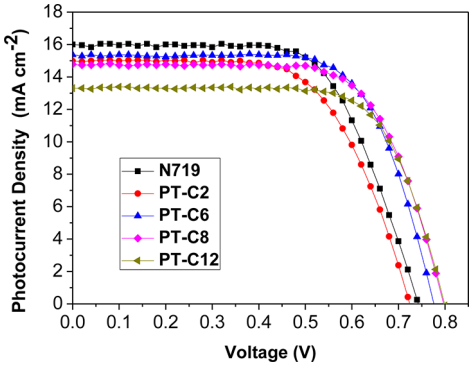

Figure 5. Photocurrent−voltage (J−V) plots obtained with the new dyes and N719.

dx.doi.org/10.1021/cm400800h | *Chem. Mater.* XXXX, XXX, XXX−XXX

attributed to the enhanced light harvesting capacity, electron lifetime, and resistance to recombination of electrons (vide infra), arising from the simple dye molecules with a dual conjugation of 4-hexyloxybenzene substituent and N(10)-hexyl chain.[15] Also, other cells sensitized with the dyes **PT-C2**, **PT-C8**, and **PT-C12** also showed attractive performances with η values of 6.87%, 8.08%, and 7.57%, respectively. It is found that the V_{oc} increases from 0.723 to 0.799 V when the chain length changed from the ethyl (**PT-C2**) to 1-dodecyl (**PT-C12**) unit. This was assigned to the reduced recombination ability at the TiO_2/dye/electrolyte interface by insulating the alkyl chains on the dyes. However, further increase in chain length resulted in decreasing η (from **PT-C6** to **PT-C8** and **PT-C12**). One reason for this evolution is that the 1-dodecyl chain is soft and twisted, and this can create hindrance for the hole transportation which retards the dye regeneration. Apparently, another consequence of the steric hindrance is that the dye loading capacity should become smaller.[34] On the other hand, the progressively reduced LUMO level usually causes the charge injection kinetics to become slower, which also contributes to the reducing trend in η.

The incident photon-current conversion efficiencies (IPCEs) for these dyes in DSSCs are plotted in Figure 6. The IPCEs of

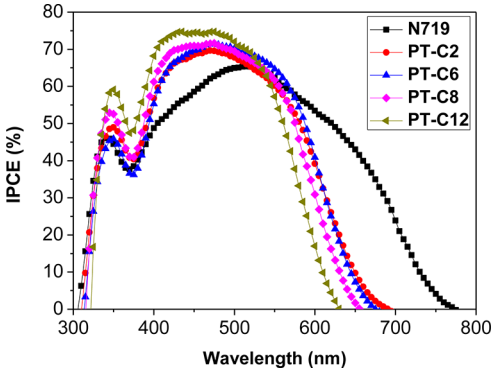

Figure 6. Incident photon-to-current efficiency (IPCE) curves of DSSCs based on the new dyes and N719.

PT-C2, **PT-C6**, and **PT-C8** dyes display a broad band in the region of 400−700 nm with values mostly >70−80% and show considerably higher peak IPCE values in the range of 300−600 nm than that of N719, implying that the structural optimization of these phenothiazine-based dyes is effective for DSSC application. It is worth noting that the IPCE spectrum of **PT-C6** based cell shows an obvious shift to the longer wavelength, which is consistent with the absorption of the dye in solution and on the TiO_2 film. Therefore, the higher and broader IPCE of the cell based on **PT-C6** leads to a higher J_{sc}, which is conducive to improve the photovoltaic performance of DSSCs. The aforementioned results further demonstrate that the addition of donor groups on the opposite side to the acceptor group can effectively increase the π-conjugation system and broaden the visible absorption spectrum in both solution and on the TiO_2 film, leading to significant performance enhancement of the DSSCs. Moreover, both the 1-hexyloxy unit of donor group and N(10)-alkyl substituents are not only beneficial to the formation of compact dye film on TiO_2 surface but also can help suppress dye aggregation and the dark current upon reducing the recombination of conduction-band electrons with the electrolyte. Furthermore, the N(10)-alkyl chains with different length and structure are applied to rationalize their influences on the cell performance.

Electrochemical impedance spectroscopy (EIS) has been performed to elucidate the interfacial charge recombination process in DSSCs based on these dyes under the dark conditions. As shown in Figure 7, a major semicircle for each

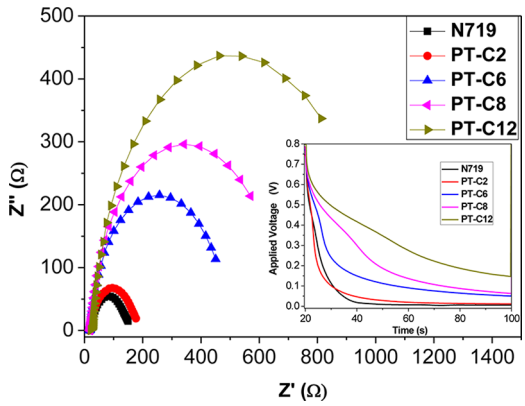

Figure 7. EIS Nyquist plots for DSSCs based on the new dyes and N719 under dark (inset: open-circuit voltage decay profiles of DSSCs based on the new dyes and N719).

dye was observed in the EIS Nyquist plot, which is related to the resistance of electron transport at the TiO_2/dye/electrolyte interface, i.e., the resistance of the recombination between electrons on the TiO_2 conduction band and I_3^- species in the electrolyte.[35] The calculated resistance values (R_{rec}) are listed in Table 2; the larger the R_{rec}, the slower the recombination kinetics. It is clear that with the increase of the chain length, from **PT-C2** to **PT-C6**, **PC-C8**, and **PT-C12**, the recombination resistance is gradually increased, which is most likely due to the increased chain length that more efficiently closes up the area for direct contact between TiO_2 and the electrolytes. On the other hand, the R_{rec} of all synthesized molecules are larger than that of N719. It can be understood as small molecules adopt dense packing on the nanoparticle surface,[36] while large molecules, such as N719, lead to more available areas for the I_3^- species diffusing onto the TiO_2 surface.[37]

To further probe the recombination kinetics of the devices, open-circuit voltage decay (OCVD) was recorded to illustrate the lifetime of V_{oc} from a steady state to dark equilibrium.[38] Figure 7 (inset) shows the OCVD profiles of devices based on these dyes. The correlation between V_{oc} decay and electron lifetime (τ_n) can be described by the following equation:

$$\tau_n = -\frac{K_B T}{e}\left(\frac{dV_{oc}}{dt}\right)^{-1}$$

where K_B is the Boltzmann constant, T is temperature, and e is the electron charge.[38,39] Therefore, the electron lifetimes can be extracted from the slope of V_{oc} decay curves. As a consequence, from devices sensitized with **PT-C12**, **PT-C8**, **PT-C6**, and **PT-C2**, the slopes become steeper and steeper, indicating that the electron lifetimes are gradually reduced with decreased length of the alkyl chain, which are well consistent with the EIS spectra that a long alkyl chain can always retard the carrier recombination. With outstanding charge separation properties at the oxide solution interface, the structural features of these phenothiazine-based dyes match the requirements for current rectification: in analogy to the photofield effect in transistors

dx.doi.org/10.1021/cm400800h | *Chem. Mater.* XXXX, XXX, XXX−XXX

and the gate for unidirectional electron flow from the electrolyte through the junction and into the oxide is opened by the photoexcitation of the sensitizer. The reverse charge flow, i.e., recapture of the electron by the electrolyte, could be impaired by a judicious design of the sensitizer.

CONCLUSIONS

In summary, a series of new simple organic dyes based on phenothiazine have been synthesized through facile modifications. The molecular design strategy here can effectively improve the efficiency of solar energy conversion which is generally determined by the light harvesting efficiency, electron injection efficiency, and undesirable charge recombination degree. These dye molecules exhibit a linear shape that is favorable for the formation of a compact sensitizer layer, while their butterfly conformations can sufficiently inhibit molecular aggregation. Also, the structural features of (4-hexyloxy)phenyl donor moiety at the C(7) position of phenothiazine extends the π-conjugation of the chromophore, therefore enhancing the performance of DSSCs. Moreover, the alkyl substituents with different chain length at the N(10) atom of phenothiazine could further optimize the performance through completely shielding the surface of TiO_2 from the I^-/I^{3-} electrolyte and subsequently reducing the leakage of dark current. Under a standard 1.5G solar illumination, the η of 8.18% based on dye **PT-C6**, which exceeds the reference Ru(II)-based N719 with an efficiency of 7.73% under the same conditions, represents the highest power conversion efficiency value when compared with the reported phenothiazine-derived dyes. The high efficiency achieved can mainly be attributed to the enhanced light harvesting capacity, electron lifetime, and resistance to recombination of electrons, arising from a simple dye molecule with a dual conjugation of 4-hexyloxybenzene substituent and *N*(10)-hexyl chain. These findings will facilitate our understanding of the crucial importance of molecular engineering and shed light on optimizing phenothiazine-based metal-free organic dyes for highly efficient DSSCs.

ASSOCIATED CONTENT

Supporting Information

Synthesis of intermediates, the open-circuit voltage decay profiles of DSSCs based on **PT-C*n*** and N719, and other spectra data of the resulted dyes (PDF). This material is available free of charge via the Internet at http://pubs.acs.org.

AUTHOR INFORMATION

Corresponding Author

*E-mail: xjzhu@hkbu.edu.hk (X.Z.); wkwong@hkbu.edu.hk (W.-K.W.); rwywong@hkbu.edu.hk (W.-Y.W.); taochen@phy.cuhk.edu.hk (T.C.). Fax: 852 3411 7348 (X.Z., W.-K.W., W.-Y.W.); 852 2603 5204 (T.C.)

Author Contributions

$^{\perp}$Y.H. and S.C. contributed equally to this work.

Notes

The authors declare no competing financial interest.

ACKNOWLEDGMENTS

We thank the National Natural Science Foundation of China (NSFC) (Grant 91222201), Hong Kong Research Grants Council (Grants HKBU202210, HKBU202811, and HKBU203011), and Hong Kong Baptist University (Grants FRG2/09-10/058, FRG2/10-11/101, and FRG2/11-12/007) for financial support. W.-K.W. and W.-Y.W. also acknowledge a grant from Areas of Excellence Scheme, University Grants Committee, Hong Kong (Project No. [AoE/P-03/08]). X.Z. and W.-Y.W. thank The Science, Technology and Innovation Committee of Shenzhen Municipality (Grants JCYJ20120829154440583 and JCYJ20120615155451326) for financial support. W.-Y.W. also thanks Dalian University of Technology for Haitian Scholarship. X.D.X and T.C. acknowledge the financial support from the CUHK Group Research Scheme and CUHK Focused Scheme B Grant "Center for Solar Energy Research".

REFERENCES

(1) O'Regan, B.; Grätzel, M. *Nature* **1991**, *353*, 737.
(2) Lewis, N. S. *Science* **2007**, *315*, 798.
(3) Chen, T.; Hu, W. H.; Song, J. L.; Guai, G. H.; Li, C. M. *Adv. Funct. Mater.* **2012**, *22*, 5245.
(4) Chang, S.; Li, Q.; Xiao, X. D.; Wong, K. Y.; Chen, T. *Energy Environ. Sci.* **2012**, *5*, 9444.
(5) Chen, T.; Guai, G. H.; Gong, C. W.; Hu, H.; Zhu, J. X.; Yang, H. B.; Yan, Q. Y.; Li, C. M. *Energy Environ. Sci.* **2012**, *5*, 6294.
(6) Yella, A.; Lee, H. W.; Tsao, H. N.; Yi, C. Y.; Chandiran, A. K.; Nazeeruddin, M. K.; Diau, E. W. G.; Yeh, C. Y.; Zakeeruddin, S. M.; Grätzel, M. *Science* **2011**, *334*, 629.
(7) Hagfeldt, A.; Boschloo, G.; Sun, L. C.; Kloo, L.; Pettersson, H. *Chem. Rev.* **2010**, *110*, 6595.
(8) Do, K.; Kim, D.; Cho, N.; Paek, S.; Song, K.; Ko, J. *Org. Lett.* **2012**, *14*, 222.
(9) Zeng, W. D.; Cao, Y. M.; Bai, Y.; Wang, Y. H.; Shi, Y. S.; Zhang, M.; Wang, F. F.; Pan, C. Y.; Wang, P. *Chem. Mater.* **2010**, *22*, 1915.
(10) Funabiki, K.; Mase, H.; Hibino, A.; Tanaka, N.; Mizuhata, N.; Sakuragi, Y.; Nakashima, A.; Yoshida, T.; Kubota, Y.; Matsui, M. *Energy Environ. Sci.* **2011**, *4*, 2186.
(11) Alibabaei, L.; Kim, J. H.; Wang, M.; Pootrakulchote, N.; Teuscher, J.; Censo, D. Di.; Humphry-Baker, R.; Moser, J. E.; Yu, Y. J.; Kay, K. Y.; Zakeeruddin, S. M.; Grätzel, M. *Energy Environ. Sci.* **2010**, *3*, 1757.
(12) Cheng, H. M.; Hsieh, W. F. *Energy Environ. Sci.* **2010**, *3*, 442.
(13) Cheng, M.; Yang, X. C.; Li, S. F.; Wang, X. N.; Sun, L. C. *Energy Environ. Sci.* **2012**, *5*, 6290.
(14) Wu, Y. Z.; Marszalek, M.; Zakeeruddin, S. M.; Zhang, Q.; Tian, H.; Gratzel, M.; Zhu, W. H. *Energy Environ. Sci.* **2012**, *5*, 8261.
(15) Ning, Z. J.; Fu, Y.; Tian, H. *Energy Environ. Sci.* **2010**, *3*, 1170.
(16) Tian, H. N.; Yang, X. C.; Chen, R. K.; Pan, Y. Z.; Li, L.; Hagfeldt, A.; Sun, L. C. *Chem. Commun.* **2007**, *43*, 3741.
(17) Wu, W. J.; Yang, J. B.; Hua, J. L.; Tang, J.; Zhang, L.; Long, Y. T.; Tian, H. *J. Mater. Chem.* **2010**, *20*, 1772.
(18) Xie, Z. B.; Midya, A.; Loh, K. P.; Adams, S.; Blackwood, D. J.; Wang, J.; Zhang, X. J.; Chen, Z. K. *Prog. Photovoltaics* **2010**, *18*, 573.
(19) Cao, D. R.; Peng, J. A.; Hong, Y. P.; Fang, X. M.; Wang, L. Y.; Meier, H. *Org. Lett.* **2011**, *13*, 1610.
(20) Chang, Y. J.; Chou, P. T.; Lin, Y. Z.; Watanabe, M.; Yang, C. J.; Chin, T. M.; Chow, T. J. *J. Mater. Chem.* **2012**, *22*, 21704.
(21) Chen, C. J.; Liao, J. Y.; Chi, Z. G.; Xu, B. J.; Zhang, X. Q.; Kuang, D. B.; Zhang, Y.; Liu, S. W.; Xu, J. R. *J. Mater. Chem.* **2012**, *22*, 8994.
(22) Kim, S. H.; Kim, H. W.; Sakong, C.; Namgoong, J.; Park, S. W.; Ko, M. J.; Lee, C. H.; Lee, W. I.; Kim, J. P. *Org. Lett.* **2011**, *13*, 5784.
(23) Zhou, G.; Pschirer; Schoneboom, J. C.; Eickemeyer, F,; Baumgarten, M,; Mullen, K. *Chem. Mater.* **2008**, *20*, 1808.
(24) Wan, Z. Q.; Jia, C. Y.; Duan, Y. D.; Zhou, L. L.; Lin, Y.; Shi, Y. *J. Mater. Chem.* **2012**, *22*, 25140.
(25) Meryer, T.; Ogermann, D.; Pankrath, A.; Kleinermanns, K.; J.Muller, T. J. *J. Org. Chem.* **2012**, *77*, 3704.
(26) Wan, Z. Q.; Jia, C. Y.; Zhang, J. Q.; Duan, Y. D.; Lin, Y.; Shi, Y. *J. Power Sources* **2012**, *199*, 426.
(27) Yang, C. J.; Chang, Y. J.; Watanabe, M.; Hon, Y. S.; Chow, T. J. *J. Mater. Chem.* **2012**, *22*, 4040.

(28) Iqbal, Z.; Wu, W. Q.; Kuang, D. B.; Wang, L. Y.; Meier, H.; Cao, D. R. *Dyes Pigm.* **2013**, *96*, 722.
(29) Nazeeruddin, M. K.; Kay, A.; Rodicio, I.; Humphry-Baker, R.; Muller, E.; Liska, P.; Vlachopoulos, N.; Grätzel, M. *J. Am. Chem. Soc.* **1993**, *115*, 6382.
(30) Kitamura, T.; Ikeda, M.; Shigaki, K.; Inoue, T.; Anderson, N. A.; Ai, X.; Lian, T. Q.; Yanagida, S. *Chem. Mater.* **2004**, *16*, 1806.
(31) Hagberg, D. P.; Edvinsson, T.; Marinado, T.; Boschloo, G.; Hagfeldt, A.; Sun, L. C. *Chem. Commun.* **2006**, *21*, 2245.
(32) Nazeeruddin, M. K.; Pechy, P.; Renouard, T.; Zakeeruddin, S. M.; Humphry-Baker, R.; Comte, P.; Liska, P.; Cevey, L.; Costa, E.; Shklover, V.; Spiccia, L.; Deacon, G. B.; Bignozzi, C. A.; Gratzel, M. *J. Am. Chem. Soc.* **2001**, *123*, 1613.
(33) Bessho, T.; Yoneda, E.; Yum, J.-H.; Guglielmi, M.; Tavernelli, I.; Imai, H.; Rothlisberger, U.; Nazeeruddin, M. K.; Grätzel, M. *J. Am. Chem. Soc.* **2009**, *131*, 5930.
(34) Hong, Y. P.; Liao, J. Y.; Fu, J. L.; Kuang, D. B.; Meier, H.; Su, C. Y.; Cao, D. R. *Dyes Pigm.* **2012**, *94*, 481.
(35) He, J. J.; Benko, G.; Korodi, F.; Polivka, T.; Lomoth, R.; Akermark, B.; Sun, L. C.; Hagfeldt, A.; Sundstrom, V. *J. Am. Chem. Soc.* **2002**, *124*, 4922.
(36) Wang, Z. S.; Cui, Y.; Dan-Oh, Y.; Kasada, C.; Shinpo, A.; Hara, K. *J. Phys. Chem. C* **2007**, *111*, 7224.
(37) Love, J. C.; Estroff, L. A.; Kriebel, J. K.; Nuzzo, R. G.; Whitesides, G. M. *Chem. Rev.* **2005**, *105*, 1103.
(38) Zaban, A.; Greenshtein, M.; Bisquert, J. *ChemPhysChem* **2003**, *4*, 859.
(39) Bisquert, J.; Zaban, A.; Greenshtein, M.; Mora-Seró, I. *J. Am. Chem. Soc.* **2004**, *126*, 13550.